© 2015. Published by The Company of Biologists Ltd | Development (2015) 142, 2653-2664 doi:10.1242/dev.124776

RESEARCH ARTICLE

# Pbx1-dependent control of VMC differentiation kinetics underlies gross renal vascular patterning

**Romulo Hurtado[1,*], Rediet Zewdu[2,*], James Mtui[1], Cindy Liang[1], Robert Aho[2], Chad Kurylo[1], Licia Selleri[2,‡,§] and Doris Herzlinger[1,‡,§]**

## ABSTRACT

The architecture of an organ's vascular bed subserves its physiological function and metabolic demands. However, the mechanisms underlying gross vascular patterning remain elusive. Using intravital dye labeling and 3D imaging, we discovered that systems-level vascular patterning in the kidney is dependent on the kinetics of vascular mural cell (VMC) differentiation. Conditional ablation of the TALE transcription factor *Pbx1* in renal VMC progenitors in the mouse led to the premature upregulation of PDGFRβ, a master initiator of VMC-blood vessel association. This precocious VMC differentiation resulted in nonproductive angiogenesis, abnormal renal arterial tree patterning and neonatal death consistent with kidney dysfunction. Notably, we establish that Pbx1 directly represses *Pdgfrb*, and demonstrate that decreased *Pdgfrb* dosage in conditional *Pbx1* mutants substantially rescues vascular patterning defects and neonatal survival. These findings identify, for the first time, an *in vivo* transcriptional regulator of PDGFRβ, and reveal a previously unappreciated role for VMCs in systems-level vascular patterning.

**KEY WORDS: Angiogenesis, Imaging, Renal development, Transcriptional regulation, Vascular mural cells, Vascular patterning, Mouse**

## INTRODUCTION

The circulatory system delivers oxygen and nutrients, and removes carbon dioxide and metabolic wastes from all tissues of the body (Johnson, 2003). Its constituent blood vessels are composed of an inner endothelial layer and an outer layer of vascular mural cells (VMCs). The endothelium serves as a semi-permeable barrier between intravascular and interstitial space and provides a non-thrombogenic surface for blood flow. The VMCs, including vascular smooth muscle and pericytes, control vessel stability and tone (Jain, 2003; Armulik et al., 2011; Hall et al., 2014).

A wealth of experimental data describes how this basic blood vessel anatomy is established during embryonic development. First, mesodermal endothelial progenitors coalesce into cords of cells that develop lumens. Vascular endothelial growth factor (VEGF) is a key signaling factor mediating this process of vasculogenesis, and many other signaling factors required for the initial stage of blood vessel formation have been elucidated (Marcelo et al., 2013). Next, the primitive endothelial tubes undergo an angiogenic phase of growth, which includes cell proliferation and branching morphogenesis controlled, in large part, by Notch signaling (Potente et al., 2011). During this stage, nascent endothelial tubes begin to recruit vascular mural cells, a process dependent on platelet-derived growth factor (PDGF) signaling (Betsholtz, 2004; Boyle et al., 2014). Specifically, endothelia secrete PDGF-BB, which activates PDGFRβ-expressing VMCs, stimulating their migration and association with the endothelial tubes (Leveen et al., 1994; Soriano, 1994; Lindahl et al., 1997; Hellstrom et al., 1999; Bjarnegård et al., 2004). Although PDGF, as well as other signaling pathways controlling the association of VMCs with nascent endothelial tubes, are well characterized (Jain, 2003), the signaling pathways and transcriptional regulation of VMC differentiation remains elusive. This is due to the varied sources of VMC progenitors and the dearth of molecular markers that identify these progenitors prior to their upregulated expression of more mature VMC markers, such as PDGFRβ or the glycoprotein NG2 (CSPG4 – Mouse Genome Informatics) (Armulik et al., 2011). Finally, after VMC incorporation, nascent blood vessels begin to mature. Maturation is essential for the generation of the semi-permeable properties of the endothelium and the formation of an extracellular matrix that provides support to vessels as they accommodate blood flow (Jain, 2003).

Although all blood vessels develop a common basic structure via angiogenic and vasculogenic processes, their three-dimensional (3D) organization differs dramatically between organs. In addition, the magnitude of blood flow into many organs, including the lung, liver and kidney, far exceeds metabolic needs. These differences in blood flow and systems-level, or gross vascular, architecture reflect the role of the circulatory system in mediating organ-specific functions. Notably, the kidney illustrates well the relationship between physiological function and gross vascular architecture (Johnson, 2003; Rector, 2007). The kidneys receive 25% of cardiac output at rest but comprise <0.4-0.5% of body mass. This magnitude of blood flow is required for the kidneys' excretory functions, and the renal vascular bed has a unique stereospecific architecture to facilitate the removal of waste from the systemic circulation. Specifically, the renal arterial tree undergoes limited branching prior to conducting virtually all of renal blood flow to the glomeruli, capillary beds that filter the blood to remove waste.

To date, the cell types and signaling pathways controlling organ systems-level vascular patterning remain elusive. This is due, in part, to the difficulty of imaging the entire vascular bed of an organ in three dimensions (Walls et al., 2008). Here, we developed techniques to analyze the 3D structure of the renal vasculature in intact embryonic mouse kidneys during development and discovered that the kinetics of renal VMC differentiation play a fundamental role in establishing the stereotypic architecture of the renal arterial tree. Previous fate-mapping experiments in both the chick and mouse embryo demonstrate that renal VMCs derive from

[1]Department of Physiology and Biophysics, Weill Cornell Medical College, New York, NY 10065, USA. [2]Department of Cell and Developmental Biology, Weill Cornell Medical College, New York, NY 10065, USA.
*These authors contributed equally to this work
‡These authors contributed equally to this work

§Authors for correspondence (lis2008@med.cornell.edu; daherzli@physbio-tech.net)

**Received 24 March 2015; Accepted 9 June 2015**

Development (2015) 142, 2653-2664 doi:10.1242/dev.124776

a mesenchymal population that selectively expresses the forkhead transcription factor Foxd1 (Guillaume et al., 2009; Humphreys et al., 2010). In this article, we establish that these renal VMC progenitors express the TALE transcription factor Pbx1 prior to their differentiation into mature VMCs. Notably, Pbx1 plays a pivotal role in promoting progenitor self-renewal/maintenance at the expense of differentiation in other cell lineages (Selleri et al., 2001; Ficara et al., 2008). Conditional *Pbx1* inactivation in the renal VMC lineage resulted in the premature differentiation of VMC progenitors into PDGFRβ$^+$ VMCs, non-productive angiogenesis, abnormal arterial branching, a marked perturbation of renal arterial tree architecture, and neonatal death consistent with kidney dysfunction. Strikingly, lowering *Pdgfrb* dosage in *Pbx1*-null VMC progenitors substantially rescued mutant vascular patterning defects and prolonged neonatal survival.

These studies identify an *in vivo* regulator of *Pdgfrb* transcription, which has yet to be elucidated despite the essential role PDGF signaling plays in vascular development. Moreover, this work establishes that tight regulation of the temporal and spatial pattern of VMC differentiation is required for renal function and for generating the stereospecific structure of the renal arterial tree. Collectively, our research uncovers a novel role for VMCs in mediating systems-level vascular patterning.

## RESULTS

### Fate mapping demonstrates that Pbx1 is expressed by VMC progenitors prior to their differentiation

Fate-mapping experiments demonstrate that Foxd1-expressing mesenchyme present at the periphery of the metanephric rudiment is a self-renewing progenitor population that gives rise to renal stroma, including VMCs (Kobayashi et al., 2014). Specifically, vascular smooth muscle, micro-vascular pericytes and glomerular pericytes (mesangial cells) all derive from Foxd1$^+$ progenitors (Fig. 1A) (Guillaume et al., 2009; Humphreys et al., 2010). To analyze the temporal and spatial pattern of VMC differentiation in the kidney, we tagged Foxd1$^+$ progenitors and their daughters by crossing a mouse line with Cre driven by the *Foxd1* promoter (*Foxd1-GC*) (Humphreys et al., 2010) to a *Rosa-YFP* reporter line (Srinivas et al., 2001). Using this breeding strategy, self-renewing VMC progenitors can be identified by Foxd1 or Cre antibody staining and YFP florescence, whereas their descendants can be identified by YFP florescence alone. The phenotype of lineage-tagged Foxd1$^+$ VMC progenitors and their daughters was analyzed by immunofluorescence (IF) throughout kidney development (Fig. 1A-P; supplementary material Fig. S1A-X).

At embryonic day (E) 11.5, when mouse kidney development initiates, Foxd1$^+$ VMC progenitors present at the periphery of the rudiment exhibited robust YFP fluorescence (Fig. 1B-D; supplementary material Fig. S1D,E). Confirming the specificity of Cre expression driven by *Foxd1* in the *Foxd1-GC* knock-in allele, neither YFP nor Cre was detected in nephron epithelia or the ureteric bud, which derive from distinct Six2$^+$ and Ret$^+$ lineages, respectively (supplementary material Fig. S1B-J) (Costantini and Kopan, 2010). Notably, lineage-tagged YFP$^+$ Foxd1$^+$ progenitors exhibited high levels of Pbx1 (Fig. 1C). Differentiated VMC markers, including PDGFRβ, NG2 and αSMA (Acta2 – Mouse Genome Informatics), were not detected in the developing kidney at this stage (Fig. 1D; supplementary material Fig. S1K,L). By E13.5, lineage-tagged self-renewing VMC progenitors (YFP$^+$, Foxd1$^+$, Pbx1$^+$ cells), persisted at the periphery of the rudiment (Fig. 1E,F; supplementary material Fig. S1F-H,J,M). Moreover, a population of YFP$^+$ VMC progenitors that have downregulated Foxd1 was interspersed between developing nephrons (Fig. 1E,F; supplementary material Fig. S1M). Differentiated vascular mural cell markers were not detected in either the self-renewing Foxd1$^+$Pbx1$^+$ VMC progenitor population or Pbx1$^+$ VMC progenitors lacking Foxd1 expression.

Lineage-tagged cells exhibiting a definitive VMC phenotype, as determined by PDGFRβ expression (Armulik et al., 2011), were first detected at E13.5. These Foxd1-derived PDGFRβ$^+$ cells or VMCs lacked Pbx1 expression (Fig. 1G,H). Moreover, lineage-tagged PDGFRβ$^+$ cells were located interior to the peripheral Foxd1 expression domain. Flow cytometry (FACS) of PDGRFβ$^+$ cells indicated that at least 85% of the PDGFRβ$^+$ cells were YFP$^+$, establishing that PDGFRβ denotes Foxd1-derived cells (supplementary material Fig. S1T). By E15.5, large populations of lineage-tagged PDGFRβ$^+$ VMCs (Fig. 1I) were present and many of them co-expressed other VMC markers, including αSMA and NG2 (supplementary material Fig. S1N-S). These lineage-tagged cells expressing differentiated VMC markers were associated with VE-Cadherin$^+$ (VECAD$^+$; Cdh5 – Mouse Genome Informatics) blood vessels and within Bowman's space, further confirming their identity as VMCs and glomerular mesangial cells, respectively (Fig. 1J; supplementary material Fig. S1N-S).

To determine whether the blood vessels associated with differentiated VMCs were competent to conduct blood, intravital dye labeling was performed using Alexa-594-Tomato Lectin (TL) to label blood-conducting vessels. Cells expressing PDGFRβ (Fig. 1K,L), NG2 and αSMA (supplementary material Fig. S1U-X), were selectively localized around blood-conducting vessels. Although many of the vessels, including the small-caliber glomerular capillaries, conducted blood, a large number of VECAD$^+$ structures lacking TL staining were observed (Fig. 1M,N). These immature, poorly perfused sinusoidal endothelial channels were associated with Pbx1$^+$ VMC progenitors lacking differentiated VMC marker expression (Fig. 1I,O). Thus, immature vessels are associated with Pbx1$^+$ VMC progenitors, but not differentiated VMCs. These data are consistent with the role of VMCs in stabilizing nascent blood vessels to accommodate blood flow (Armulik et al., 2011). Quantitative analyses demonstrated that all lineage-tagged VMC progenitors were Foxd1$^+$Pbx1$^+$PDGFRβ$^-$ at E11.5, whereas at least 85% of their descendants were Foxd1$^-$Pbx1$^-$PDGFRβ$^+$ by E18.5 (Fig. 1P). Thus, Pbx1 is expressed by VMC progenitors prior to their differentiation and upregulation of PDGFRβ and other well-characterized VMC markers. Our data, showing that Pbx1 downregulation is associated with upregulated PDGFRβ expression, raised the possibility that Pbx1 might restrain the differentiation of VMC progenitors into definitive VMCs during early kidney development, similar to the reported role of Pbx1 in controlling differentiation of the hematopoietic and chondrocyte lineages (Selleri et al., 2001; Ficara et al., 2008).

### *Pbx1* loss of function in VMC progenitors perturbs their differentiation

To test whether Pbx1 plays a role in controlling VMC differentiation, *Pbx1* was conditionally ablated in the VMC lineage by crossing *Foxd1-GC* mice with a *Pbx1* conditional mouse strain (*Pbx1*$^{f/f}$) (Koss et al., 2012). Cre-mediated *Pbx1* excision was efficient as determined by the absence of Pbx1 in the Foxd1-VMC lineage in *Pbx1*$^{f/f}$;*Foxd1*$^{GC/+}$ embryos, hereafter referred to as *Pbx1*$^{CKO}$ (supplementary material Fig. S2A-J). As expected, Pbx1 levels were not perturbed in Pax2$^+$ nephron progenitors or ureteral mesenchyme, which derive from distinct Six2 and Tbx18 lineages, respectively (supplementary material Fig. S2I,J) (Kobayashi et al., 2008; Bohnenpoll et al., 2013).

Development (2015) 142, 2653-2664 doi:10.1242/dev.124776

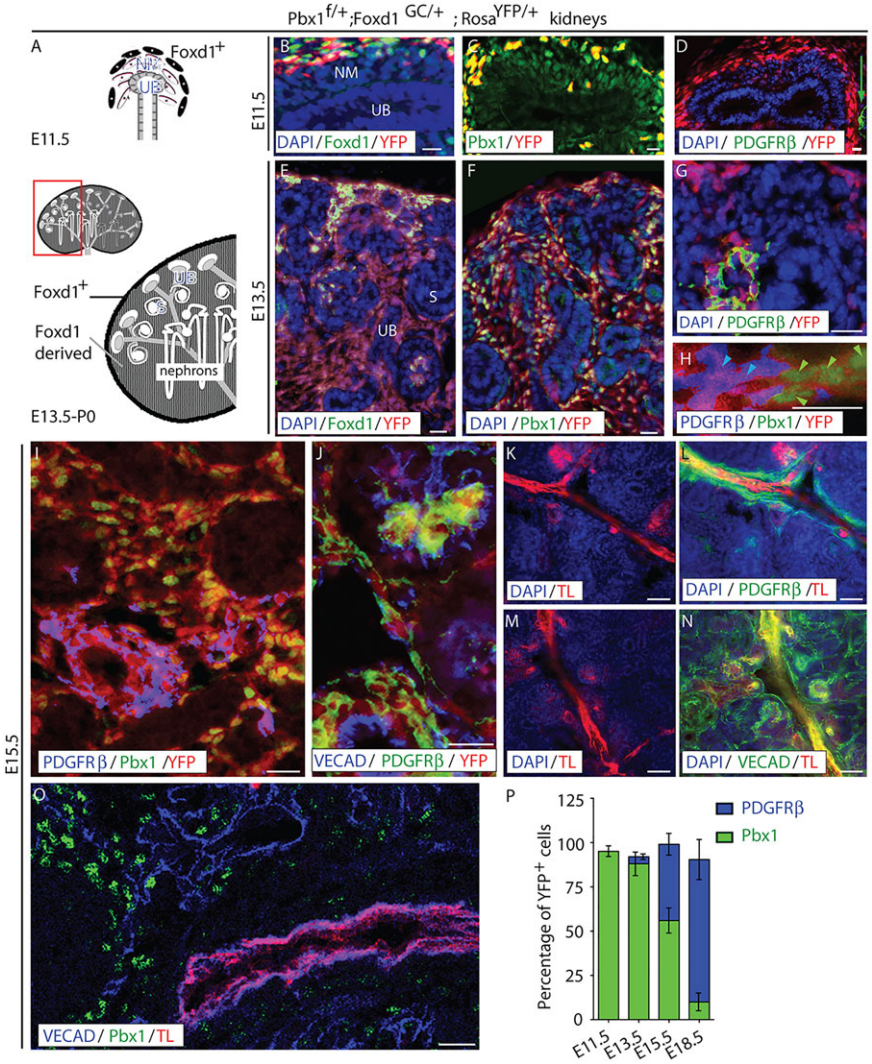


**Fig. 1. Pbx1 is expressed by VMC progenitors prior to their differentiation.** (A) Diagram of the tissues forming the developing kidney at the initiation of kidney development (E11.5, top) and at later stages of development (E13.5-P0, bottom). The E11.5 kidney rudiment includes renal epithelial progenitors, including the ureteric bud (UB), nephrogenic mesenchyme (NM) and peripheral Foxd1$^{+}$ mesenchyme, which gives rise to VMCs. Later in development, a population of self-renewing Foxd1$^{+}$ VMC-progenitors persists at the periphery of the kidney, whereas Foxd1-derived progeny are located within the interstitial compartment between developing S-shaped body and more mature nephrons. (B-J) Frozen sections of kidneys from *Pbx1$^{fl/+}$; Foxd1$^{GC/+}$; Rosa$^{YFP/+}$* embryos in which YFP is expressed in all cells derived from Foxd1$^{+}$-VMC progenitors. E11.5 (B-D), E13.5 (E-H) and E15.5 (I,J) renal tissues were assayed by IF for the detection of Foxd1 (B,E), Pbx1 (C,F,H,I), PDGFRβ (D,G,H,I,J) and VE-cadherin (VECAD; J). The self-renewing VMC progenitor population was identified by co-expression of Foxd1 and YFP fluorescence, VMC progenitors by YFP fluorescence, and definitive Foxd1-derived VMCs by PDGFRβ and YFP expression. VECAD staining was used to visualize vascular endothelia. At E11.5 (B), the vast majority of Foxd1$^{+}$ progenitors located at the periphery of the rudiment express the YFP lineage tag (D) and Pbx1 (C). Differentiated VMCs, as determined by PDGFRβ$^{+}$ expression, are not present in the kidney at this stage, although they can be seen in extra-renal tissues (D, green arrow). At E13.5, cells co-expressing Foxd1$^{+}$ and Pbx1 remain localized to the periphery of the rudiment (E), whereas their Pbx1$^{+}$ progeny, which have downregulated Foxd1, are present in the interstitial compartment (F). At this stage, small populations of lineage-tagged cells expressing PDGFRβ are observed (G,H). These differentiated VMCs lack Pbx1 (H; green arrowheads indicate Pbx1$^{+}$YFP$^{+}$ nuclei; light blue arrowheads indicate PDGFRβ$^{+}$YFP$^{+}$ VMCs). At E15.5, large populations of differentiated PDGFRβ$^{+}$Pbx1$^{-}$ lineage-tagged VMCs are observed (I). These cells are localized around blood vessels (J), further confirming their VMC phenotype. Scale bars: 10 µm. (K-O) E15.5 kidneys processed by intravital dye labeling using Tomato Lectin (TL) to label blood-conducting vessels (K-O) and subsequent IF detection of PDGFRβ (L), VECAD (N,O) and Pbx1 (O). PDGFRβ$^{+}$ VMCs are selectively associated with mature, blood-conducting vessels, whereas the majority of VECAD$^{+}$ cords and vessels are associated with VMC progenitors that have yet to differentiate. Scale bars: 50 µm. (P) Quantification of the percentage of YFP$^{+}$ Foxd1 progeny expressing Pbx1 or PDGFRβ at different stages of development ($n \geq 3$ genotype/stage). Error bars represent s.d. See also supplementary material Fig. S1.

*Pbx1$^{CKO}$* embryos were retrieved at the expected Mendelian ratio demonstrating that conditional *Pbx1* ablation, unlike germline *Pbx1* deletion (Selleri et al., 2001), did not compromise embryogenesis. However, *Pbx1$^{CKO}$* pups failed to thrive after birth and survived 1 day to 4 weeks. Blood chemistry revealed a threefold elevation in the blood-urea-nitrogen (BUN)/creatinine ratio in *Pbx1$^{CKO}$* pups compared with *Pbx1$^{f/+}$;Foxd1$^{GC/+}$* littermates, hereafter referred to as *Pbx1$^{Ctrl}$* (supplementary material Fig. S2K). Notably, elevated BUN/creatinine ratios indicate renal failure and can be caused by abnormalities in pre-glomerular renal blood flow, which is modulated by VMC tone (Johnson, 2003; Rector, 2007).

Strikingly, gross defects in VMC differentiation were observed in mutant embryos as early as E13.5 (Fig. 2A-K). In control *Pbx1$^{f/+}$; Foxd1$^{GC/+}$;Rosa$^{YFP/+}$*, hereafter called *Pbx1$^{Ctrl}$;Rosa$^{YFP}$* kidneys,

Development (2015) 142, 2653-2664 doi:10.1242/dev.124776

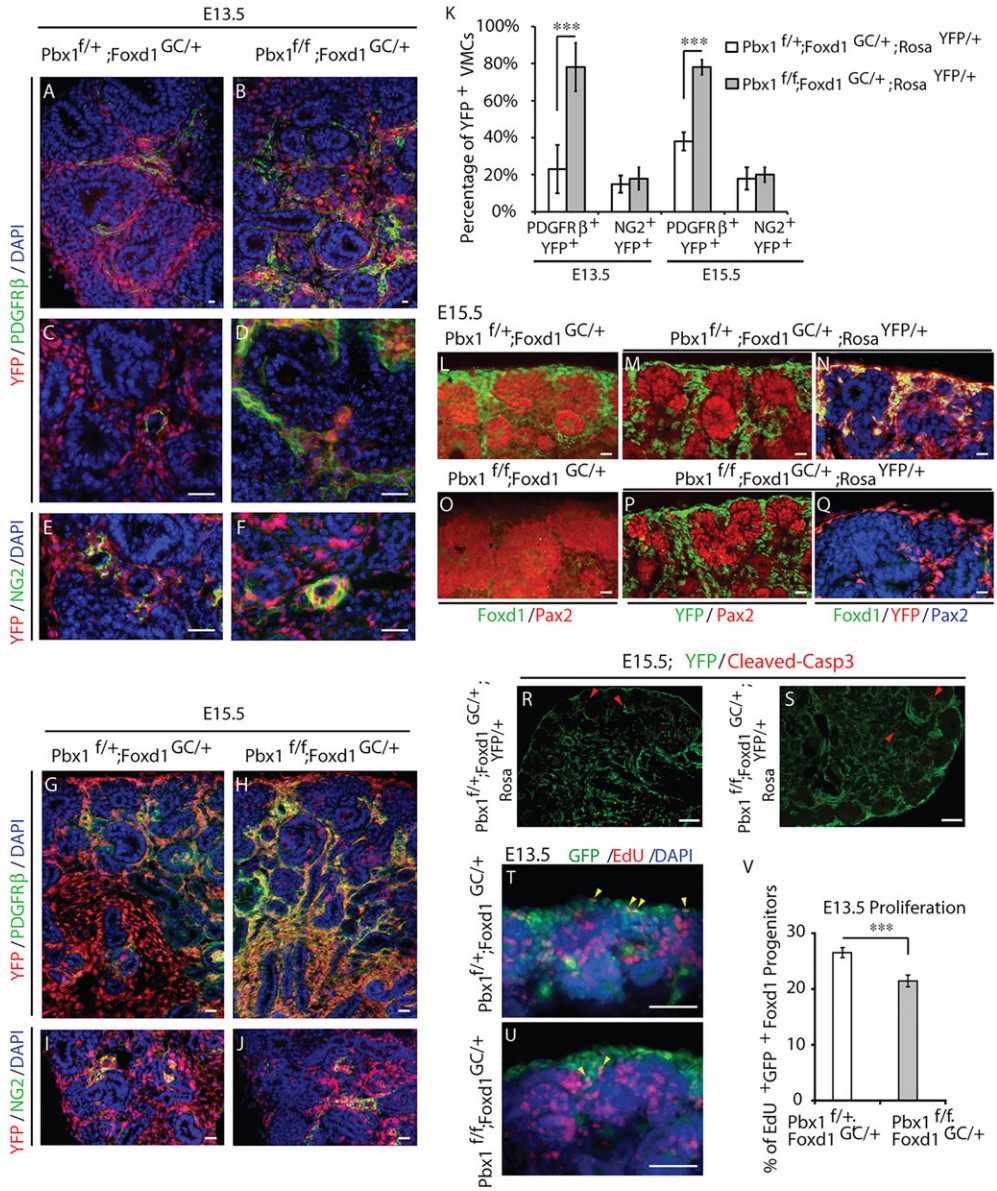


**Fig. 2. Foxd1-Cre-mediated *Pbx1* excision results in ectopic and precocious upregulation of PDGFRβ in the VMC lineage and premature depletion of self-renewing VMC progenitors.** (A-J) Control *Pbx1*$^{fl/+}$; *Foxd1*$^{GC/+}$; *Rosa*$^{YFP/+}$ (A,C,E,G,I) and mutant *Pbx1*$^{fl/f}$; *Foxd1*$^{GC/+}$;*Rosa*$^{YFP/+}$ (B,D,F,H,J) kidneys analyzed at E13.5 (A-F) and E15.5 (G-J) by IF for the detection of PDGFRβ (A-D,G,H) and NG2 (E,F,I,J). Foxd1 derivatives were identified by YFP fluorescence. Inactivation of *Pbx1* in the VMC lineage results in precocious and ectopic PDGFRβ expression in VMCs. The expression of the VMC marker NG2 is not dysregulated by *Pbx1* inactivation. Scale bars: 10 µm. (K) Quantification of the percentage of YFP$^+$ Foxd1 derivatives expressing PDGFRβ or NG2 present in control *Pbx1*$^{fl/+}$;*Foxd1*$^{GC/+}$;*Rosa*$^{YFP/+}$ and mutant *Pbx1*$^{fl/f}$;*Foxd1*$^{GC/+}$;*Rosa*$^{YFP/+}$ kidneys at E13.5 and E15.5. *n*=4 embryos per genotype at each stage of development; error bars represent s.d. ***$P$<0.001. (L-Q) IF detection of Foxd1$^+$ VMC progenitors in E15.5 control *Pbx1*$^{fl/+}$;*Foxd1*$^{GC/+}$;*Rosa*$^{YFP/+}$ (L) and mutant *Pbx1*$^{fl/f}$;*Foxd1*$^{GC/+}$;*Rosa*$^{YFP/+}$ (O) kidneys. E15.5 control *Pbx1*$^{fl/+}$;*Foxd1*$^{GC/+}$;*Rosa*$^{YFP/+}$ (M,N) and mutant *Pbx1*$^{fl/f}$;*Foxd1*$^{GC/+}$;*Rosa*$^{YFP/+}$ (P,Q) kidneys processed by IF for the detection of Pax2 (L-Q) and Foxd1 (L,N,O,Q). Foxd1-derived cells were identified by YFP fluorescence (M,N,P,Q). Self-renewing Foxd1$^+$ VMC progenitors are prematurely depleted in mutant *Pbx1*$^{fl/f}$;*Foxd1*$^{GC/+}$;*Rosa*$^{YFP/+}$ kidneys (O). Scale bars: 10 µm. (R,S) Analysis of apoptosis by IF of cleaved caspase 3 in control *Pbx1*$^{fl/+}$;*Foxd1*$^{GC/+}$;*Rosa*$^{YFP/+}$ and mutant *Pbx1*$^{fl/f}$;*Foxd1*$^{GC/+}$;*Rosa*$^{YFP/+}$ E15.5 kidneys (*n*=2 per genotype). Red arrowheads indicate apoptotic cells, which were all YFP$^-$. Scale bars: 50 µm. (T,U) Fluorescence detection of proliferating EdU$^+$ self-renewing Foxd1$^+$ progenitors in E13.5 kidneys (yellow arrowheads). Scale bars: 50 µm. (V) Mean percentages of EdU-incorporating Foxd1-GFP$^+$ cells in control E13.5 *Pbx1*$^{fl/+}$;*Foxd1*$^{GC/+}$ and mutant *Pbx1*$^{fl/f}$;*Foxd1*$^{GC/+}$ kidneys. (*n*=3 embryos per group), error bars represent s.e.m. ***$P$=0.0008. See also supplementary material Fig. S2.

PDGFRβ was detected in ~25% and 40% of the lineage-tagged Foxd1-derivatives at E13.5 and E15.5, respectively (Fig. 2A,C,G,K). By contrast, PDGFRβ was detected in 80% of the Foxd1-derivatives in mutant kidneys, hereafter called *Pbx1*$^{CKO}$;*Rosa*$^{YFP}$, at these stages (Fig. 2B,D,H,K). Such a high percentage of YFP$^+$ cells expressing PDGFRβ was not reached in control kidneys until E18.5 (Fig. 1P). Moreover, in controls (Fig. 2G), PDGFRβ$^+$ cells were restricted to the cortex, whereas they were present between tubules throughout the cortical and medullary regions in *Pbx1*$^{CKO}$;*Rosa*$^{YFP}$ kidneys (Fig. 2H). FACS analysis confirmed that the ectopic VMCs in *Pbx1*$^{CKO}$;*Rosa*$^{YFP}$ kidneys were derived from Foxd1 progenitors, similar to VMCs in control kidneys (supplementary material Fig. S2L). Unexpectedly, the percentage of Foxd1-derivatives expressing NG2, another marker of differentiated VMCs (Armulik

Development (2015) 142, 2653-2664 doi:10.1242/dev.124776

et al., 2011), was not elevated in mutant kidneys (Fig. 2E,F,I,J,K). Collectively, these data demonstrate that *Pbx1* in VMC progenitors is essential for the partial execution of VMC differentiation programs and plays a crucial role in controlling PDGFRβ temporal and spatial expression patterns.

### Pbx1 in the Foxd1 lineage is essential for VMC progenitor maintenance, but is not required for nephrogenesis

Subsequently, we tested whether the accelerated appearance of PDGFRβ$^+$ cells in *Pbx1*$^{CKO}$;*Rosa*$^{YFP}$ kidneys was associated with a premature depletion of self-renewing Foxd1$^+$-VMC progenitors. This population persists in wild-type kidneys until birth (Hatini et al., 1996; Levinson et al., 2005). As expected, Foxd1$^+$ cells were present at the periphery of E15.5 control kidneys overlying Pax2$^+$ renal epithelial progenitors (Fig. 2L-N). Although YFP$^+$ lineage-tagged cells were present at the periphery of the mutant kidney, they did not express Foxd1 (Fig. 2O-Q). Analyses of cell death assessed by immunodetection of activated caspase3 at E13.5 and E15.5 demonstrated that Foxd1$^+$ progenitor depletion in *Pbx1*$^{CKO}$ kidneys was not due to increased apoptosis (Fig. 2R,S; supplementary material Fig. S2M). Quantification of the cycling rate of Foxd1$^+$ cells at E13.5 showed a 19% reduction in *Pbx1*$^{CKO}$ kidneys relative to controls (Fig. 2T-V). Thus, Pbx1-dependent control of VMC progenitor differentiation and proliferation is essential for maintaining the self-renewing Foxd1$^+$ VMC progenitor pool.

Notably, the defects in VMC progenitor maintenance and differentiation in *Pbx1*$^{CKO}$ kidneys did not grossly perturb renal epithelial development. Specifically, both *Pbx1*$^{Ctrl}$ and *Pbx1*$^{CKO}$ embryonic kidneys exhibited robust ureteric bud branching and nephron progenitor expansion (Fig. 3A-J). By E18.5, kidneys of both genotypes exhibited an abundance of nephrons with glomerular, proximal and collecting duct nephron segments identified by IF staining for nephron segment-specific markers (Fig. 3E-J) (Jande et al., 1981; Rodman et al., 1986; Sawada et al., 1986; Zimmerhackl et al., 1996). Starting at E17.5, *Pbx1*$^{CKO}$ kidneys appeared to be smaller than controls, owing in part to a decrease in the size of the medullary interstitial compartment (supplementary material Fig. S3). By P0, *Pbx1*$^{CKO}$ kidneys were ∼30% smaller than controls (Fig. 3K). Collectively, these data establish that Pbx1 expression in VMCs is essential for VMC progenitor maintenance and differentiation, but not for nephrogenesis or collecting system morphogenesis.

### *Pbx1* ablation in VMCs perturbs renal arterial patterning

*In vitro* and *in vivo* experiments demonstrate that the association of VMCs with nascent endothelial tubes is dependent, in large part, on PDGF signaling (Leveen et al., 1994; Soriano, 1994). Specifically, PDGFRβ$^+$ VMCs migrate towards endothelia, which secrete the PDGFRβ ligand PDGF-B. Thus, it is possible that ectopic and premature PDGFRβ expression in *Pbx1*$^{CKO}$ kidneys results in the premature association of VMCs with the developing renal vascular bed. To test this hypothesis, we analyzed the percentage of the renal vascular bed associated with PDGFRβ$^+$ cells in *Pbx1*$^{Ctrl}$ and *Pbx1*$^{CKO}$ kidneys. *Pbx1* ablation in the VMC lineage did not perturb vasculogenesis as shown by the abundance of VECAD$^+$ cords and vessels in both genotypes at E13.5 (Fig. 4A-I) and E16.5 (Fig. 4J-R). However, the percentage of the total VECAD$^+$ vascular bed that is associated with PDGFRβ$^+$ cells was increased twofold in *Pbx1*$^{CKO}$ kidneys (Fig. 4E,I,N,R) compared with controls (Fig. 4A,I,J,R). Because the association of VMCs with endothelium promotes vessel maturation and efficient blood conduction, we next tested whether there were differences in the pattern of blood flow in *Pbx1*$^{CKO}$ versus *Pbx1*$^{Ctrl}$ kidneys. In *Pbx1*$^{Ctrl}$ kidneys, intravital dye labeling with

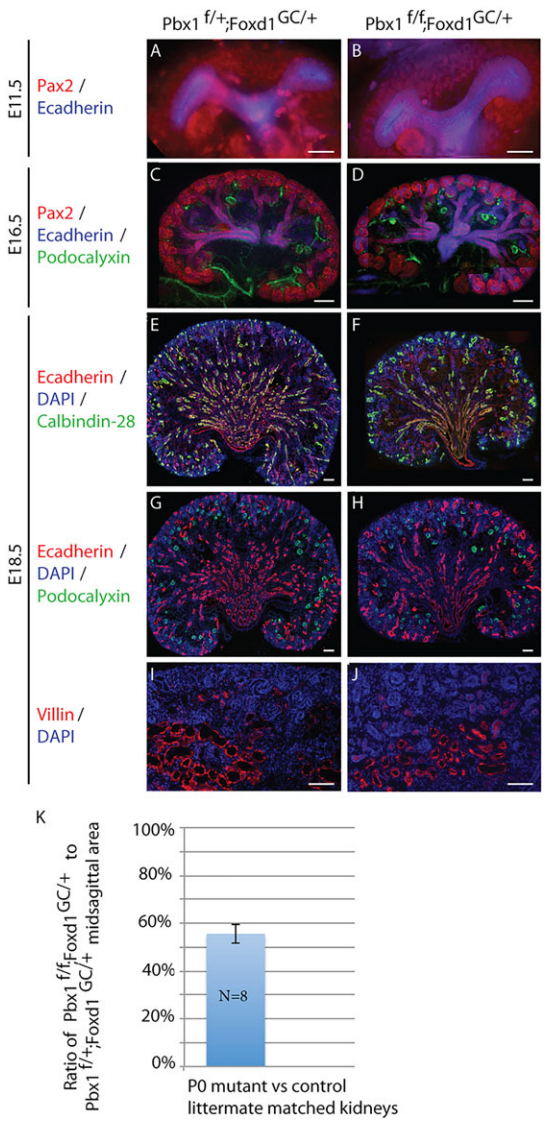


**Fig. 3. VMC lineage-specific inactivation of *Pbx1* does not affect nephrogenesis.** (A-J) Control *Pbx1*$^{fl/+}$;*Foxd1*$^{GC/+}$ and mutant *Pbx1*$^{fl/f}$;*Foxd1*$^{GC/+}$ kidneys at E11.5 (A,B), E16.5 (C,D) and E18.5 (E-J) assayed by IF for the detection of Pax2$^+$ renal epithelial progenitors (A-D), E-cadherin$^+$ (Cdh1 – Mouse Genome Informatics) renal epithelia (A-H); podocalyxin$^+$ glomerular podocytes (C,D,G,H); calbindin-28K$^+$ distal nephron segments (E,F); and villin$^+$ proximal tubules (I,J). Scale bars: 50 µm. At E11.5 (A,B) both mutant and control kidneys are characterized by a T-shaped ureteric bud surrounded by nephrogenic mesenchyme, and by E16.5 (C,D) extensive ureteric bud branching and expansion of the nephrogenic progenitor population can be seen in both genotypes. At E18.5, differentiated glomerular (G,H), proximal (I,J) and distal (E,F) nephron segments are detected in both mutant and control kidneys. (K) Although mutant kidneys exhibit well-differentiated nephrons and cortical-medullary patterning, they are ∼30% smaller than controls as determined by quantitative measurement of midsagittal area at P0. (*n*=8 per genotype; error bars represent s.d.). See also supplementary material Fig. S3.

TL, combined with VECAD IF, demonstrated that ∼25% of the VECAD$^+$ vascular bed conducted blood at E13.5 (Fig. 4B,I) and E16.5 (Fig. 4K,R). By contrast, ∼65% of the vessels in the *Pbx1*$^{CKO}$ vascular bed conducted blood at these stages (Fig. 4F,I,O,R). Next, arterial vessels that conducted blood in intact E13.5 and E16.5 *Pbx1*$^{Ctrl}$ and *Pbx1*$^{CKO}$ kidneys were analyzed in three dimensions subsequent to intravital dye labeling with TL. The control renal arterial tree followed a stereotypical pattern (Fig. 4C,D,L,M) with a

Development (2015) 142, 2653-2664 doi:10.1242/dev.124776

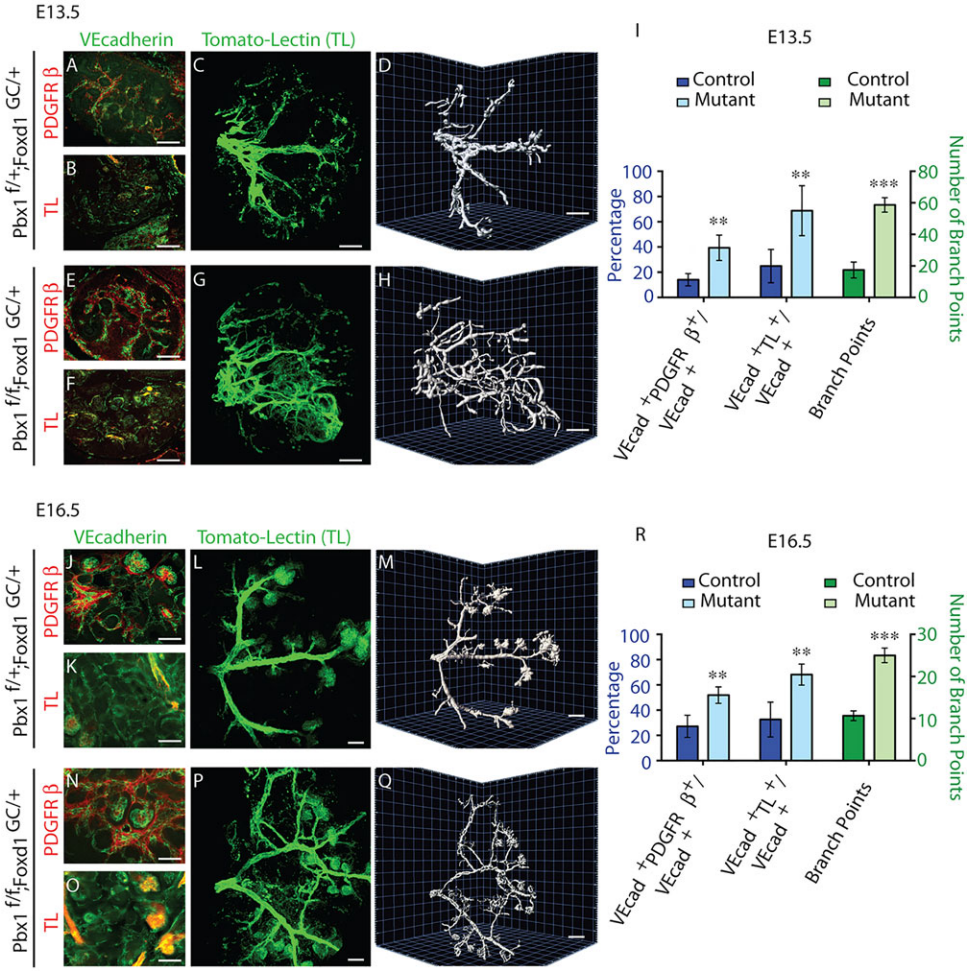


**Fig. 4. *Pbx1* in the Foxd1-VMC lineage is essential for arterial patterning.** (A-H,J-Q) E13.5 (A-H) and E16.5 (J-Q) control *Pbx1*$^{f/+}$;*Foxd1*$^{GC/+}$ (A-D,J-M) and mutant *Pbx1*$^{f/f}$;*Foxd1*$^{GC/+}$ (E-H,N-Q) kidneys processed by IF (A,B,E,F,J,K,N,O) for the detection of PDGFRβ (A,E,J,N) and VE-Cadherin (A,B,E,F,J,K,N,O). Intravital labeling with TL was used to label blood-conducting vessels. IF analyses of kidney sections subsequent to intravital dye labeling (B,F,K,O). To determine the gross architecture of the renal arterial tree, intravital dye labeling was performed with TL, and blood-conducting vessels were subsequently analyzed in three dimensions in intact kidneys. C,G,L,P are planar images; D,H,M,Q show 3D rendering. *n*>3 per genotype. Scale bars: 50 µm. (I,R) Quantification of the area of the VECAD$^+$ vascular network associated with PDGFRβ$^+$ cells (PDGFRβ$^+$/VECAD$^+$); area of the VECAD$^+$ vascular network that conducts blood (TL$^+$/VECAD$^+$); and arterial branch points (mean±s.d.); *n*>3 per genotype; ***P*<0.01, ****P*<0.001.

central renal artery giving rise to three to four major branches that extend to the cortical region of the organ, where glomeruli are located. By contrast, the organization of arterial blood vessels in *Pbx1*$^{CKO}$ kidneys was markedly perturbed (Fig. 4G,H,P,Q). Instead of the stereotypical hierarchical pattern exhibited by *Pbx1*$^{Ctrl}$ kidneys, the *Pbx1*$^{CKO}$ kidney arterial tree displayed a seemingly stochastic pattern marked by a threefold increase in arterial branching (Fig. 4G,H,P,Q,I,R). These data establish that *Pbx1* ablation causes premature upregulation of PDGFRβ in VMC progenitors, premature association of PDGFRβ$^+$ cells with the developing vascular bed, and perturbation of the stereotypic branching pattern of the renal arterial tree.

### Recruitment of Pbx transcription factors to a *Pdgfrb* cis-regulatory element represses *Pdgfrb* transcription in the developing kidney

*In situ* hybridization (ISH) on kidney sections and qRT-PCR analyses of *Pdgfrb* transcript levels from FACS-sorted YFP$^+$ cells isolated from E15.5 *Pbx1*$^{Ctrl}$;*Rosa*$^{YFP}$ and *Pbx1*$^{CKO}$;*Rosa*$^{YFP}$ kidneys showed that *Pbx1* loss in the Foxd1 lineage markedly perturbs the spatial distribution and levels of *Pdgfrb* mRNA (Fig. 5A,B). Notably, the *Pdgfrb* genomic locus harbors multiple TGACAG sequences, which are potential Pbx-Meis/Prep binding sites (Fig. 5C; supplementary material Fig. S4) (Ferretti et al., 2011; Koss et al., 2012; Penkov et al., 2013). Among these, we identified three non-coding DNA segments (E1, E2, E3) within the 5′ end of the *Pdgfrb* locus with the highest cross-species sequence conservation and/or displaying DNaseI hypersensitive sites (HS) indicative of open chromatin (Fig. 5C) (Vierstra et al., 2014). Chromatin immunoprecipitation (ChIP) assays were performed to determine whether Pbx1 binds to these regions *in vivo*. ChIP-qPCR on chromatin derived from E15.5 wild-type kidneys with a pan-Pbx antibody showed significant and striking Pbx enrichment on the DNA segment closest to the *Pdgfrb* transcriptional start site (TSS), designated as E1. A minor, albeit statistically significant, Pbx enrichment was also detected on E2, but not on E3 or other control elements lacking sequence conservation and Pbx1 binding sites (Fig. 5C,D). These findings demonstrated that the *Pdgfrb* non-coding regions E1 and E2, containing potential Pbx-Meis/Prep binding sites (TGACAG), are direct targets of Pbx binding in the developing kidney.

Subsequently, to test whether Pbx1 directly represses *Pdgfrb* transcription, luciferase reporter assays were conducted by transfecting a pGL3-TK reporter vector containing the wild-type E1 element upstream of a thymidine kinase (TK) promoter-driven *luciferase* gene into HEK293T cells. These experiments showed consistent and profound repressive effect of E1 on firefly luciferase expression (Fig. 5E). Furthermore, co-transfection of *Pbx1b* and its cofactor *Prep1* (*Pknox1* – Mouse Genome Informatics) (Ferretti et al., 1999) expression vectors resulted in a threefold enhancement of E1 repressive activity over empty vector (Fig. 5E). The repressive activity of E1 that was observed without Pbx1 overexpression is consistent with the presence of high levels of endogenous Pbx1a and Pbx1b proteins in most cell lines, including HEK-293T and NIH-3T3 cells (Fig. 5F). In contrast to the strong repressive activity

Development (2015) 142, 2653-2664 doi:10.1242/dev.124776

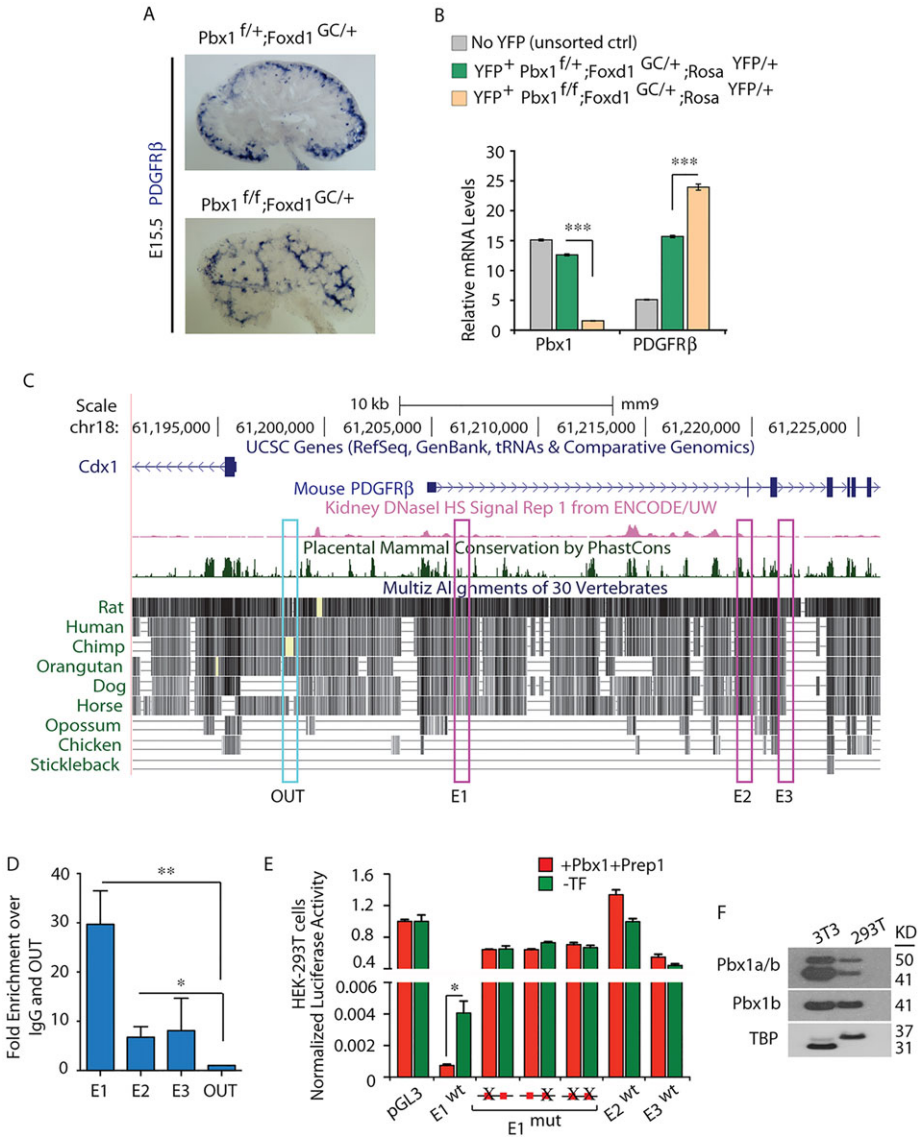


**Fig. 5. Pbx1 homeoprotein regulates *Pdgfrb* by binding to a cis-regulatory element within the *Pdgfrb* locus.** (A) ISH of *Pdgfrb* on E15.5 control *Pbx1*$^{fl/+}$;*Foxd1*$^{GC/+}$ and mutant *Pbx1*$^{fl/f}$;*Foxd1*$^{GC/+}$ kidney sections displaying ectopic *Pdgfrb* mRNA distribution in the mutant kidneys. (B) Loss of *Pbx1* in the Foxd1 lineage results in upregulation of *Pdgfrb* transcript levels. Quantitative RT-PCR analysis of *Pdgfrb* and *Pbx1* mRNAs in FACS-sorted YFP$^{+}$ cells obtained from E15.5 *Pbx1*$^{fl/+}$;*Foxd1*$^{GC/+}$;*Rosa*$^{YFP/+}$ and *Pbx1*$^{fl/f}$;*Foxd1*$^{GC/+}$;*Rosa*$^{YFP/+}$ and cells from control YFP$^{-}$ kidneys. Values were normalized to the housekeeping gene *Tbp*. Kidney cells were pooled from at least five embryos per genotype. The experiment was performed in technical triplicates. Error bars represent s.e.m.; ***$P$<0.0001. (C) 5′ portion of the mouse *Pdgfrb* locus (UCSC Genome Browser, mm9). Conservation plot across vertebrate species; dark green peaks indicate highest conservation across mammals; pink peaks indicate sites of open chromatin by the presence of DNaseI hypersensitivity; pink boxes (E1, E2, E3) highlight conserved non-coding regions containing consensus Pbx-Meis/Prep binding sequences. (D) ChIP-qPCR of Pbx binding to two *Pdgfrb* cis-regulatory regions in E15.5 wild-type kidneys. Fold enrichment over IgG relative to amplification within a non-conserved region (OUT) is shown. Error bars represent s.e.m. from six IPs with an anti-PanPbx antibody from two independent chromatin preparations. Significant binding of Pbx to E1 (**$P$=0.0018) and E2 (*$P$=0.025) was observed. (E) Pbx-dependent transcription reporter assays in HEK-293T cells transfected with the indicated plasmids. Representative experiment (out of eight) is shown. Data were calculated as firefly to *Renilla* luciferase ratios of each reporter construct, normalized to empty TK-pGL3 firefly to *Renilla* ratios (set to 1). Wild-type (wt) E1 strongly repressed firefly luciferase expression, which is significantly enhanced upon Pbx1b and Prep1 overexpression (cumulative *$P$=0.011). Disruption of one or both Pbx-Meis/Prep binding motifs in E1 abrogated transcriptional repressive activity. Activities of E2 and E3 were negligible. (F) Immunoblot revealing endogenous Pbx1a and Pbx1b proteins in 293T and 3T3 cell lines. TBP, loading control. See also supplementary material Fig. S4.

of E1, E2 and E3 had neutral or less marked effects on luciferase transcription (Fig. 5E). Crucially, transcriptional repression of luciferase was largely abolished when mutated E1 (in which one or both Pbx-Meis/Prep TGACAG motifs were mutated to GCAATG) was inserted into pGL3-TK (Fig. 5E). Collectively, these findings established the requirement of Pbx1 for the repression of *Pdgfrb* transcription in the developing kidney *in vivo*, via Pbx binding to the *Pdgfrb* cis-regulatory element E1.

## Genetic ablation of one *Pdgfrb* allele partially rescues mutant vascular patterning and neonatal survival in *Pbx1*$^{CKO}$ mice

If the loss of Pbx1-mediated *Pdgfrb* repression underlies the abnormal renal phenotypes observed in mutant kidneys, decreasing *Pdgfrb* gene dosage in *Pbx1*$^{CKO}$ embryos would be expected to rescue the mutant kidney phenotype. Accordingly, we crossed *Pbx1*$^{f/f}$;*PDGFRβ*$^{f/+}$ with *Pbx1*$^{f/+}$;*Foxd1*$^{GC/+}$ mice to generate

Development (2015) 142, 2653-2664 doi:10.1242/dev.124776

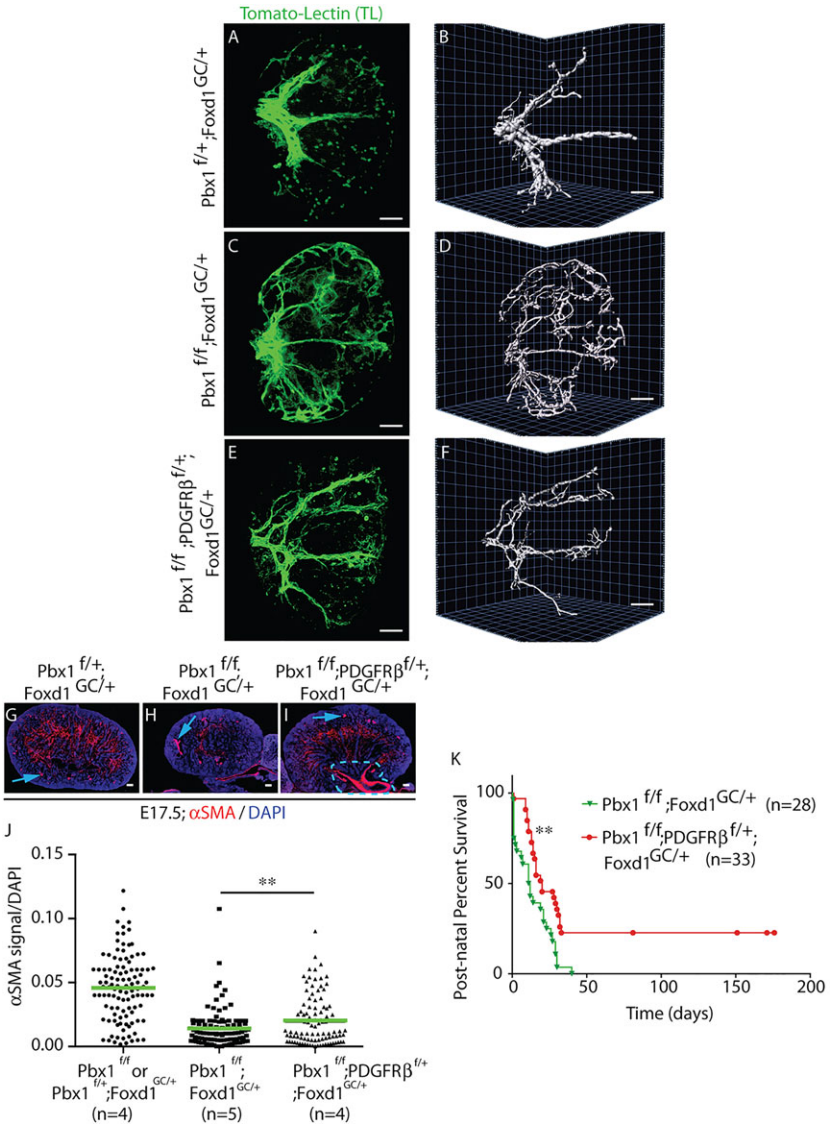


**Fig. 6. Loss of one *Pdgfrb* allele partially rescues kidney vascular defects, interstitial expansion and survival in mutants lacking Pbx1 in the VMC lineage.** (A-F) Labeling of blood-conducting vessels by intravital dye labeling with TL in whole E13.5 kidneys from control *Pbx1*$^{f/+}$;*Foxd1*$^{GC/+}$ (A,B), mutant *Pbx1*$^{f/f}$;*Foxd1*$^{GC/+}$ (C,D) and *PDGFRβ*$^{het}$ rescue *Pbx1*$^{f/f}$;*PDGFRβ*$^{f/+}$;*Foxd1*$^{GC/+}$ (E,F) embryos (*n*=3 per genotype). A,C,E are planar images and B,D,F show 3D rendering. Scale bars: 50 µm. (G-I) Representative IF images of interstitial αSMA in E17.5 control *Pbx1*$^{f/+}$; *Foxd1*$^{GC/+}$, mutant *Pbx1*$^{f/f}$;*Foxd1*$^{GC/+}$ and rescue *Pbx1*$^{f/f}$; *PDGFRβ*$^{f/+}$;*Foxd1*$^{GC/+}$ kidney sections. Blood vessels (blue arrows) and ureteric smooth muscle (blue outline) αSMA$^{+}$ compartments were masked out in quantitative analysis (shown in J). Scale bars: 50 µm. (J) Scatter dot plots representing the αSMA$^{+}$ medullary interstitium as a ratio of total DAPI signal in serial kidney sections of the three genotypes, analyzed by Matlab. Green lines indicate mean values. A total of ~100 kidney sections from four to five kidneys per genotype were analyzed. ***P*=0.0099. (K) Kaplan–Meier plots showing significantly improved (***P*=0.0014) post-natal survival of *PDGFRβ*$^{het}$ rescue mice compared with mutant *Pbx1*$^{f/f}$;*Foxd1*$^{GC/+}$ neonates as assessed by the standard Log-rank test. See also supplementary material Fig. S5.

littermate *Pbx1*$^{CKO}$, *Pbx1*$^{f/+}$;*PDGFRβ*$^{f/+}$;*Foxd1*$^{GC/+}$ and *Pbx1*$^{f/f}$; *PDGFRβ*$^{f/+}$;*Foxd1*$^{GC/+}$, hereafter named *PDGFRβ*$^{het}$ rescue embryos (Fig. 6). Inactivation of one allele of *Pdgfrb* by Foxd1-Cre was sufficient to reduce *Pdgfrb* mRNA levels in *Pbx1*$^{f/+}$; *PDGFRβ*$^{f/+}$;*Foxd1*$^{GC/+}$ kidneys by 45% compared with controls (supplementary material Fig. S5A). Strikingly, the renal vascular patterning defects of *Pbx1*$^{CKO}$ kidneys were significantly rescued in *PDGFRβ*$^{het}$ rescue kidneys (Fig. 6A-F). Consistent with results shown in Fig. 4, 3D analysis of the renal arterial blood vessels in E13.5 control kidneys (Fig. 6A,B) showed a stereotypical organization of a central renal artery forming three to four major branches, whereas *Pbx1*$^{CKO}$ kidneys (Fig. 6C,D) exhibited an abnormal, stochastic arterial blood vessel pattern. By contrast, the pattern of the arterial vasculature in E13.5 *PDGFRβ*$^{het}$ rescue kidneys (Fig. 6E,F) resembled that of control kidneys with a central renal artery giving rise to major blood vessels that extend to the cortical region of the organ. Indeed, the rescue in blood vessel patterning was marked by a partial normalization in arterial branching. As previously observed, *Pbx1*$^{CKO}$ kidneys displayed a threefold increase in arterial branching (Fig. 4I,R) relative to controls, whereas *PDGFRβ*$^{het}$ rescue kidneys showed only a 1.5-fold increase (supplementary material Fig. S5B). In addition, unlike E17.5 control kidneys (Fig. 6G), *Pbx1*$^{CKO}$ kidneys typically showed a dramatically decreased domain of αSMA$^{+}$ medullary interstitium (Fig. 6H). By contrast, *PDGFRβ*$^{het}$ rescue kidneys (Fig. 6I) exhibited an expanded medullary interstitial αSMA$^{+}$ domain similar to that of controls (Fig. 6G) with a 1.45-fold increase in interstitial αSMA$^{+}$ domain compared with *Pbx1*$^{CKO}$ kidneys (Fig. 6J). Lastly, postnatal survival of *PDGFRβ*$^{het}$ rescue mice was also significantly prolonged (median survival: 20 days) compared with *Pbx1*$^{CKO}$ mice (median survival: 11.5 days) (Fig. 6K). Together, the substantial rescue of the mutant *Pbx1*$^{CKO}$ kidney phenotype by decreasing PDGFRβ levels establishes that Pbx1-dependent *Pdgfrb* transcriptional repression is an essential mechanism underlying the reported *Pbx1*$^{CKO}$ kidney phenotypes.

## DISCUSSION

We have discovered that Pbx1 homeodomain protein is a crucial repressor of *Pdgfrb* transcription in the developing kidney. In the absence of *Pbx1*, the maturation of VMC progenitors is perturbed, as shown by an accelerated acquisition of the VMC marker PDGFRβ, at the expense of the progenitor marker Foxd1. In addition, we have demonstrated that the pattern of the renal arterial tree is disrupted in embryonic kidneys by *Pbx1* loss in the VMC

Development (2015) 142, 2653-2664 doi:10.1242/dev.124776

lineage. Genetic rescue experiments via deletion of one allele of *Pdgfrb* in *Pbx1*$^{CKO}$ kidneys significantly restored renal arterial patterning, αSMA$^{+}$ medullary interstitial expansion and survival. Collectively, these data establish that *Pdgfrb* repression *in vivo* is Pbx1 dependent and that the number, spatial distribution and temporal appearance of PDGFRβ$^{+}$ VMCs play a crucial role in patterning the vascular and interstitial components of the developing kidney (Fig. 7).

Although much progress has been made in elucidating the molecular control of endothelial tube assembly, lumen formation and sprouting during the angiogenic phase of blood vessel development, the molecular mechanisms that control systems-level vascular patterning remain poorly understood. Notably, the gross architecture of an organ's vascular bed is essential for its physiological functions (Mahadevan et al., 2014), a relationship that is well illustrated in the kidney (Sequeira-Lopez and Gomez, 2011). Renal excretory functions are dependent on the delivery of 25% of cardiac output directly to the glomerular capillaries, which filter blood to remove waste. Accordingly, the renal arterial tree exhibits a hierarchical architecture that undergoes limited branching. Our data reveal that loss of *Pbx1* in VMCs results in marked perturbation of arterial patterning. Specifically, *Pbx1*$^{CKO}$ kidneys exhibited a threefold increase in arterial branching, compared with controls. As a result of increased tortuosity introduced by this non-productive angiogenesis, blood flow can become turbulent (Johnson, 2003) in certain areas of the arterial bed of *Pbx1*$^{CKO}$ kidneys. This, in turn, would lead to a decrease in blood flow rate and a drop in glomerular filtration pressure, which could increase plasma BUN/creatinine ratios. Consistent with this model, *Pbx1*$^{CKO}$ mutants had a threefold increase in BUN/creatinine ratios, compared with controls. Thus, the formation of a functional renal arterial tree is dependent on Pbx1-directed transcriptional programs in renal VMCs.

Here, we determine that the vascular patterning defects in *Pbx1*$^{CKO}$ kidneys are due to the essential role that Pbx1 plays in regulating VMC differentiation. Interestingly, previous research has established that *Pbx1* loss of function causes abnormal cardiovascular development, including severe edema, and pallor from impaired vascularization resulting in late gestational lethality (Selleri et al., 2001). Moreover, compound loss of multiple Pbx genes results in vascular patterning defects, such as abnormal morphogenesis of the great arteries (Chang et al., 2008; Stankunas et al., 2008). However, these reports did not explore whether Pbx proteins and their cofactors affect vascular development through cell autonomous or non-cell autonomous mechanisms, nor did they identify which Pbx-dependent pathways were perturbed, questions we have addressed in the present study. We demonstrate here that vascular abnormalities in kidneys lacking *Pbx1* in the Foxd1-dervied VMC lineage (*Pbx1*$^{CKO}$) are non-cell autonomous and are linked to aberrant upregulation of PDGFRβ and subsequent premature and ectopic association of PDGFRβ$^{+}$ VMCs with nascent vessels. Because VMCs play a fundamental role in vessel stabilization, we hypothesize that the premature increase in VMC number and ectopic VMC localization in mutants results in premature vessel stabilization at ectopic sites within the kidney. This premature and ectopic vessel stabilization is likely to antagonize vessel remodeling, which includes the pruning of vessel branches lacking adequate blood flow. Alternatively, it is possible that the increased number of VMCs actually increases vessel branching and is independent of the role of VMCs in vessel stabilization.

PDGFRβ is a receptor tyrosine kinase that is selectively expressed by VMCs and interstitial mesenchymal cells in kidney and other organs (Armulik et al., 2011). Various organs, including the kidney, from *Pdgfrb*$^{-/-}$ and *Pdgfb*$^{-/-}$ late-stage embryos manifest a gross reduction in VMC abundance, resulting in enlarged and leaky hemorrhagic vessels (Hellstrom et al., 2001). These and other loss-of-function studies established that PDGFRβ signaling is essential for the recruitment of VMCs to PDGFB$^{+}$ endothelium and is essential for maturation and stabilization of developing vessels to accommodate blood flow (Lindahl et al., 1997; Hellstrom et al., 1999; Bjarnegård et al., 2004; Armulik et al., 2011). Additionally, knock-in of a constitutively active *Pdgfrb* allele resulted in an excess of VMCs, which was associated with abnormal vessel diameter and wall thickness (Magnusson et al., 2007; Olson and Soriano, 2011). Moreover, PDGFRβ$^{+}$ cells in mice with constitutively activated PDGFRβ exhibited abnormal differentiation potential, such as marked downregulation of contractile proteins, including αSMA, together with enhanced expression of inflammatory signature genes (Olson and Soriano, 2011). Overall, in addition to these loss-of-function and gain-of-function phenotypes, our study establishes that not only is the appropriate dosage of PDGFRβ crucial for vascular development, but so is its correct spatial and temporal expression during kidney development. Specifically, we demonstrated that in the *Pbx1*$^{CKO}$ kidney the untimely and ectopic upregulation of *Pdgfrb* is associated with the formation of excess VMCs, leading to an abnormal renal arterial network, a deficit of αSMA$^{+}$ interstitium, and loss of normal kidney function.

Despite the crucial role of PDGFRβ in VMC function and vascular patterning during embryogenesis, not many factors that regulate its transcription have been identified *in vivo*. Several transcription factors (TFs) are known to activate or repress *Pdgfrb* in cell culture systems; however, the biological function of *Pdgfrb* regulation by these TFs *in vivo* remains elusive (Ballagi et al., 1995; Uramoto et al., 2004; Jin et al., 2008; Weissmueller et al., 2014). In the present study, we show

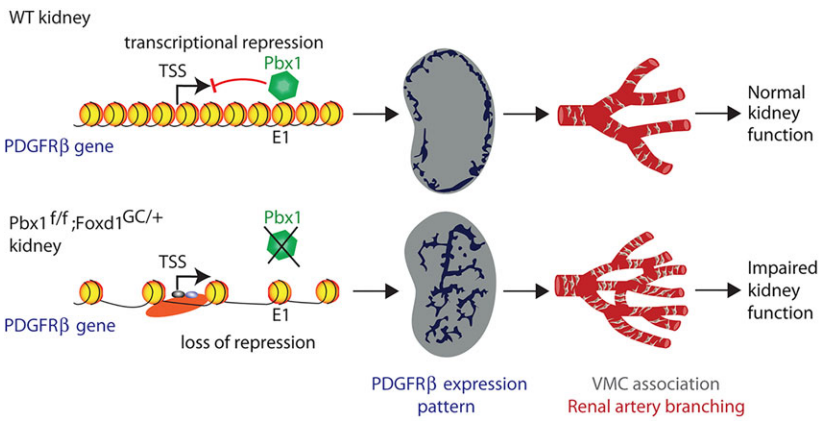


**Fig. 7. Model for Pbx1-dependent vascular patterning in the developing kidney.** In wild-type (WT) kidney, during the initial stages of renal development, Pbx1 binds the E1 cis-regulatory element of *Pdgfrb*, repressing transcription and spatially restricting its expression to cortical domains of the kidney. As a result, the temporal and spatial association of VMCs with the developing vasculature is tightly regulated leading to the normal hierarchical pattern of the renal arterial network required for renal function. By contrast, in *Pbx1*$^{f/f}$;*Foxd1*$^{GC/+}$ kidneys, *Pdgfrb* repression is released in the VMC progenitors. This de-repression results in precocious and ectopic *Pdgfrb* expression in VMCs, the premature association of PDGFRβ$^{+}$ VMCs with the nascent vascular bed, abnormal arterial branching, impaired renal function and neonatal demise.

Development (2015) 142, 2653-2664 doi:10.1242/dev.124776

that in the developing kidney, Pbx binds a regulatory element of *Pdgfrb in vivo* and suppresses its transcription. Owing to this repressive activity, Pbx controls the kinetics of *Pdgfrb* expression in the Foxd1 lineage as it differentiates into VMCs. Members of the Pbx-Meis/Prep family of TALE homeodomain TFs are mostly described as positive regulators of transcription. However, we have recently demonstrated Pbx-dependent repression of the cell cycle inhibitor gene *Cdkn2b* (Koss et al., 2012) and the osteoblast-related gene *Osx* (*Sp7* – Mouse Genome Informatics) (Gordon et al., 2010). Notably, recent reports suggest the ability of Pbx to interact with and recruit co-repressors, including Hdac1 (part of the Sin3/NuRD/Co-REST regulatory complex) and Hdac3 (part of the NCoR/SMRT complex), which facilitate chromatin condensation by histone 3 deacetylation and nucleosome positioning (Asahara et al., 1999; Chariot et al., 1999; Saleh et al., 2000; Choe et al., 2009; Gordon et al., 2010). Thus, it is possible that similar mechanisms of Pbx1-dependent repression are used to regulate *Pdgfrb* transcription in the developing kidney.

We demonstrate here that dysregulation of *Pdgfrb* transcription underlies the $Pbx1^{CKO}$ kidney phenotypes in embryos with Foxd1 lineage-specific *Pbx1* loss. As complete inactivation of *Pdgfrb* causes massive loss of VMCs, resulting in additional kidney defects (Soriano, 1994; Hellstrom et al., 1999; Tallquist et al., 2003), it was feasible to delete only one *Pdgfrb* allele. Remarkably, this was sufficient to obtain a significant rescue of the $Pbx1^{CKO}$ kidney phenotypes, including vascular patterning, medullary stromal expansion and survival after birth. Although additional Pbx1 target genes might be concomitantly dysregulated in the *Pbx1*-deficient Foxd1 lineage, our results underscore the prominent role of Pbx1-directed control of *Pdgfrb* transcription in the developing kidney, a process that remains poorly understood.

Understanding the transcriptional regulation of *Pdgfrb* is of high clinical significance. Specifically, organ fibrosis, which is mediated by dysregulated VMC proliferation and differentiation (Bonner, 2004; Humphreys et al., 2010; Goritz et al., 2011), can be experimentally induced by the activation of PDGFRβ signaling (Floege et al., 1993; Tang et al., 1996). Furthermore, VMCs have recently emerged as attractive therapeutic targets for pathologies with dysfunctional vasculature or tissue scarring (Schrimpf and Duffield, 2011; Ruan et al., 2013). Accordingly, our study identifying Pbx1 as a new regulator of VMC homeostasis has important implications for human diseases with VMC perturbations. Thus, Pbx1 can be a potential target for attenuating PDGFRβ signaling and the progression of fibrosis. In pathological conditions such as diabetic retinopathy and tumorigenesis, capillary beds exhibit compromised vessel integrity and leakiness, which is linked to VMC detachment and deficiency (Bergers and Song, 2005). Increasing VMC coverage of blood vessels may treat these conditions. Therefore, Pbx1 inactivation and subsequent transcriptional de-repression of *Pdgfrb* has the potential to promote VMC recruitment and vessel stabilization in these diseases.

## MATERIALS AND METHODS

### Mice

The mouse lines used in these studies have been previously described by our and other laboratories: *Pbx1* conditional mice (Koss et al., 2012), *Foxd1-GFP-Cre* (Humphreys et al., 2010), *R26-stop-eYFP* (Srinivas et al., 2001) and *Pdgfrb* conditional mice (Olson and Soriano, 2011).

### Immunofluorescence, *in situ* hybridization, western blot and antibodies

For IF, frozen sections (10 µm) of E11.5-E18.5 kidneys were prepared and processed for IF as described (Hurtado and Mikawa, 2006; Ferretti et al., 2011). Primary antibody binding was detected by AlexaFluor-conjugated secondary antibodies (Molecular Probes) and nuclei were stained with either DAPI (Sigma) or TO-PRO-3 (Invitrogen).

ISH was performed as previously described (Hurtado and Mikawa, 2006). The *Pdgfrb* ISH probe plasmid, described by Lindahl et al. (1997), was obtained from P. Soriano (Icahn School of Medicine, NY, USA). *Foxd1/BF-2* ISH probe plasmid was described by Hatini et al. (1996).

For western blotting, nuclear extracts were prepared from 293T and 3T3 cells in membrane lysis buffer (250 mM sucrose, 20 mM HEPES pH 7.4, 10 mM KCl, 1.5 mM $MgCl_2$, 1 mM EDTA, 1 mM EGTA, protease inhibitor cocktail), followed by pelleting of nuclei and incubation in RIPA buffer and sonication on ice for 5 minutes. Equal amounts of proteins (30 µg) were subjected to SDS-PAGE with 4-12% (v/v) Bis-Tris gels (Invitrogen). Proteins were transferred onto PVDF membranes (Millipore). Subsequently, standard immunoblotting was performed with antibodies against Pbx1a/b (Cell Signaling Technology 4342), Pbx1b (sc101852, Santa Cruz Biotechnology) and TBP (Cell Signaling Technology 8515).

See supplementary materials and methods for details of primary antibodies.

### Intravital dye labeling and 3D imaging

The embryonic renal arterial vessels conducting blood were analyzed in three dimensions by intravital dye labeling with tomato lectin (TL) (Vector Laboratories), and subsequent imaging of intact kidneys. Briefly, 20 µl of TL (0.2 mg/ml) was injected into the embryonic circulation by cardiac puncture. After 5 min of incubating embryos at 37°C+5% $CO_2$, whole kidneys were isolated and formaldehyde-fixed, and subsequently cleared using the ClearT2 method (Kuwajima et al., 2013). Whole kidneys were imaged in their intact form using confocal microscopy, and then analyzed in three dimensions using Imaris Imaging Software (Bitplane).

### Analysis of cell proliferation

E13.5 pregnant mice were injected intraperitoneally with EdU (5-ethynyl-2′-deoxyuridine; Invitrogen) at 50 mg/kg body weight and embryos were retrieved 1 hour later. Kidneys were isolated and prepared for cryosectioning as described above. Sections were collected at 50-µm intervals, and $Foxd1^+$ progenitors present in *Foxd1-GC* mice were detected by IF using anti-GFP. Subsequently, Click-iT EdU chemistry (Invitrogen) was performed to detect DNA-incorporated EdU with Alexa Fluor 594-conjugated azide according to the manufacturer's instructions. $GFP^+EdU^+$/total $GFP^+$ nuclei or proliferation rates were calculated in ImageJ from three embryos of each genotype.

### i-STAT Serum Measurements

Postnatal day (P) 23 pups were anesthetized and blood was drawn using intracardiac puncture. Approximately 100 µl of blood was injected into i-STAT EC8+ and iSTAT Crea cartridges (Abbot Laboratories) for determination of glucose, urea nitrogen (BUN), creatinine hemoglobin, hematocrit, pH, Na, K, Cl, $TCO_2$, $HCO_3$, $PCO_2$, Anion Gap and Base Excess. All measurements were made on littermates of $Pbx1^{Ctrl}$ and $Pbx1^{CKO}$ mice.

### FACS cytometry and sorting

E15.5 kidneys were dissociated into single cell suspensions by incubation in collagenase IV (2.5 mg/ml), dispase II (2.5 mg/ml) (both from Roche), DNaseI (0.1 mg/ml) (Stem Cell Technologies), 5% fetal bovine serum, 25 mM HEPES pH 7.4 in HBSS for 30 minutes at 37°C. Subsequently, cells were washed in HBSS containing 1% FBS and 2 mM EDTA to inactivate collagenase, and filtered through a 70-µm nylon mesh. DAPI (0.2 µg/ml) was used to exclude dead cells. Samples were run on FACSAriaII-SORP (Becton Dickinson) at Weill Cornell Flow Cytometry Core following standard procedures. Data were analyzed using BD FACSDiva Software. $YFP^-$ cells were used as controls for determining gates.

### Quantitative real-time PCR

Total RNA and cDNA were generated from E15.5 FACS-sorted kidney cells. RNA was isolated using the RNeasy Kit (Qiagen). RNA was treated with RNase-free DNase (Qiagen). cDNA was prepared using the Superscript

Development (2015) 142, 2653-2664 doi:10.1242/dev.124776

III First-Strand Synthesis System (Invitrogen). Quantitative RT-PCR was performed on cDNA samples utilizing ABI Universal PCR Master Mix (Applied Biosystems) and was run on a TaqMan 7900HT real-time PCR machine (Applied Biosystems). The TaqMan Gene Expression assays and oligonucleotides are listed in supplementary materials and methods.

### Chromatin immunoprecipitation

Approximately 200 kidneys were dissected in PBS/PMSF from E15.5 embryos and processed for ChIP as described (Ferretti et al., 2011; Vitobello et al., 2011). The primers used to detect conserved elements (E1, E2, E3) and a control region outside of the conserved regions (OUT) following standard PCR conditions on ABI 7900HT machine (Applied Biosystems) are listed in supplementary materials and methods.

### Transcriptional reporter assays

A heterologous promoter, pGL3 reporter vector (Promega) in which putative regulatory elements in *Pdgfrb* locus were cloned upstream of a thymidine kinase (TK) promoter, was transiently transfected into 293T, 3T3 cells using FuGENE HD Transfection reagent (Roche) following the manufacturer's instructions. In addition, *Renilla* luciferase plasmid (Promega) for transfection control and *Pbx1b* and *Prep1* expression vectors or an equivalent amount of empty *pcDNA.3-lacZ* expression vector were co-transfected as appropriate. Primers used for cloning of the putative regulatory regions identified in the *Pdgfrb* locus into the pGL3-TK reporter vector as well as for mutagenesis of region E1 are listed in supplementary materials and methods.

Transient transfections in HEK293T cells were performed using protocols reported by Koss et al. (2012).

### Statistical analysis

For analysis of quantitative data, datasets were compared using unpaired two-tailed Student's *t*-tests with $P<0.05$ considered significant. Kaplan–Meier curves and associated statistical tests were executed using GraphPad Prism software. Programming of algorithms for quantification and modeling of $\alpha SMA^{+}$ medullary stroma in E17.5 kidneys were performed using Matlab software (MathWorks). The threshold for determination of accepted signal was calculated for each section by determining the min/max algorithm.

### Fluorescence microscopy and image acquisition

Wide-field fluorescence imaging was performed on a Zeiss Axioplan2 upright microscope, captured using a Hamamatsu Orca camera, and acquired using the Open Lab software (PerkinElmer). Confocal imaging was performed on an inverted Leica DMI 600 microscope, captured using a Leica HyD detector, and acquired using the Leica LAS Software.

#### Acknowledgements

We thank Elizabeth Lacy, Todd Evans, Lauretta Lacko, Allison North, Sina Rabbany, Arthur Kilduff and James Hart for advice; and Philippe Soriano for the generous sharing of probes. We thank Jason McCormick at WCMC's Flow Cytometry Core for FACS analysis.

#### Competing interests

The authors declare no competing or financial interests.

#### Author contributions

R.H. and R.Z. designed experiments, performed experiments and data analysis, and co-wrote the manuscript; J.M., C.L. and C.K., performed experiments; R.A. performed image analyses by Matlab; L.S. developed the concept, performed data analyses and co-wrote the manuscript; D.H. developed the concept, performed experiments and data analysis, and co-wrote the manuscript.

#### Funding

This work was supported by the National Institutes of Health [R01 DK45218 and R01 DK08723 to D.H.; R01 HD061403 to L.S.]. Deposited in PMC for release after 12 months.

#### Supplementary material

Supplementary material available online at
http://dev.biologists.org/lookup/suppl/doi:10.1242/dev.124776/-/DC1

#### References

**Armulik, A., Genové, G. and Betsholtz, C.** (2011). Pericytes: developmental, physiological, and pathological perspectives, problems, and promises. *Dev. Cell* **21**, 193-215.

**Asahara, H., Dutta, S., Kao, H.-Y., Evans, R. M. and Montminy, M.** (1999). Pbx-Hox heterodimers recruit coactivator-corepressor complexes in an isoform-specific manner. *Mol. Cell. Biol.* **19**, 8219-8225.

**Ballagi, A. E., Ishizaki, A., Nehlin, J.-O. and Funa, K.** (1995). Isolation and characterization of the mouse PDGF β-receptor promoter. *Biochem. Biophys. Res. Commun.* **210**, 165-173.

**Bergers, G. and Song, S.** (2005). The role of pericytes in blood-vessel formation and maintenance. *Neurooncology* **7**, 452-464.

**Betsholtz, C.** (2004). Insight into the physiological functions of PDGF through genetic studies in mice. *Cytokine Growth Factor Rev.* **15**, 215-228.

**Bjarnegård, M., Enge, M., Norlin, J., Gustafsdottir, S., Fredriksson, S., Abramsson, A., Takemoto, M., Gustafsson, E., Fässler, R. and Betsholtz, C.** (2004). Endothelium-specific ablation of PDGFB leads to pericyte loss and glomerular, cardiac and placental abnormalities. *Development* **131**, 1847-1857.

**Bohnenpoll, T., Bettenhausen, E., Weiss, A.-C., Foik, A. B., Trowe, M.-O., Blank, P., Airik, R. and Kispert, A.** (2013). *Tbx18* expression demarcates multipotent precursor populations in the developing urogenital system but is exclusively required within the ureteric mesenchymal lineage to suppress a renal stromal fate. *Dev. Biol.* **380**, 25-36.

**Bonner, J. C.** (2004). Regulation of PDGF and its receptors in fibrotic diseases. *Cytokine Growth Factor Rev.* **15**, 255-273.

**Boyle, S. C., Liu, Z. and Kopan, R.** (2014). Notch signaling is required for the formation of mesangial cells from a stromal mesenchyme precursor during kidney development. *Development* **141**, 346-354.

**Chang, C.-P., Stankunas, K., Shang, C., Kao, S.-C., Twu, K. Y. and Cleary, M. L.** (2008). Pbx1 functions in distinct regulatory networks to pattern the great arteries and cardiac outflow tract. *Development* **135**, 3577-3586.

**Chariot, A., van Lint, C., Chapelier, M., Gielen, J., Merville, M.-P. and Bours, V.** (1999). CBP and histone deacetylase inhibition enhance the transactivation potential of the HOXB7 homeodomain-containing protein. *Oncogene* **18**, 4007-4014.

**Choe, S.-K., Lu, P., Nakamura, M., Lee, J. and Sagerström, C. G.** (2009). Meis cofactors control HDAC and CBP accessibility at Hox-regulated promoters during zebrafish embryogenesis. *Dev. Cell* **17**, 561-567.

**Costantini, F. and Kopan, R.** (2010). Patterning a complex organ: branching morphogenesis and nephron segmentation in kidney development. *Dev. Cell* **18**, 698-712.

**Ferretti, E., Schulz, H., Talarico, D., Blasi, F. and Berthelsen, J.** (1999). The PBX-regulating protein PREP1 is present in different PBX-complexed forms in mouse. *Mech. Dev.* **83**, 53-64.

**Ferretti, E., Li, B., Zewdu, R., Wells, V., Hebert, J. M., Karner, C., Anderson, M. J., Williams, T., Dixon, J., Dixon, M. J. et al.** (2011). A conserved Pbx-Wnt-p63-Irf6 regulatory module controls face morphogenesis by promoting epithelial apoptosis. *Dev. Cell* **21**, 627-641.

**Ficara, F., Murphy, M. J., Lin, M. and Cleary, M. L.** (2008). Pbx1 regulates self-renewal of long-term hematopoietic stem cells by maintaining their quiescence. *Cell Stem Cell* **2**, 484-496.

**Floege, J., Eng, E., Young, B. A., Alpers, C. E., Barrett, T. B., Bowen-Pope, D. F. and Johnson, R. J.** (1993). Infusion of platelet-derived growth factor or basic fibroblast growth factor induces selective glomerular mesangial cell proliferation and matrix accumulation in rats. *J. Clin. Invest.* **92**, 2952.

**Gordon, J. A. R., Hassan, M. Q., Saini, S., Montecino, M., van Wijnen, A. J., Stein, G. S., Stein, J. L. and Lian, J. B.** (2010). Pbx1 represses osteoblastogenesis by blocking Hoxa10-mediated recruitment of chromatin remodeling factors. *Mol. Cell. Biol.* **30**, 3531-3541.

**Goritz, C., Dias, D. O., Tomilin, N., Barbacid, M., Shupliakov, O. and Frisen, J.** (2011). A pericyte origin of spinal cord scar tissue. *Science* **333**, 238-242.

**Guillaume, R., Bressan, M. and Herzlinger, D.** (2009). Paraxial mesoderm contributes stromal cells to the developing kidney. *Dev. Biol.* **329**, 169-175.

**Hall, C. N., Reynell, C., Gesslein, B., Hamilton, N. B., Mishra, A., Sutherland, B. A., O'Farrell, F. M., Buchan, A. M., Lauritzen, M. and Attwell, D.** (2014). Capillary pericytes regulate cerebral blood flow in health and disease. *Nature* **508**, 55-60.

**Hatini, V., Huh, S. O., Herzlinger, D., Soares, V. C. and Lai, E.** (1996). Essential role of stromal mesenchyme in kidney morphogenesis revealed by targeted disruption of Winged Helix transcription factor BF-2. *Genes Dev.* **10**, 1467-1478.

**Hellstrom, M., Lindahl, P., Abramsson, A. and Betsholtz, C.** (1999). Role of PDGF-B and PDGFR-beta in recruitment of vascular smooth muscle cells and pericytes during embryonic blood vessel formation in the mouse. *Development* **126**, 3047-3055.

**Hellstrom, M., Gerhardt, H., Kalen, M., Li, X., Eriksson, U., Wolburg, H. and Betsholtz, C.** (2001). Lack of pericytes leads to endothelial hyperplasia and abnormal vascular morphogenesis. *J. Cell Biol.* **153**, 543-554.

**Humphreys, B. D., Lin, S.-L., Kobayashi, A., Hudson, T. E., Nowlin, B. T., Bonventre, J. V., Valerius, M. T., McMahon, A. P. and Duffield, J. S.** (2010).

Development (2015) 142, 2653-2664 doi:10.1242/dev.124776

Fate tracing reveals the pericyte and not epithelial origin of myofibroblasts in kidney fibrosis. *Am. J. Pathol.* **176**, 85-97.

**Hurtado, R. and Mikawa, T.** (2006). Enhanced sensitivity and stability in two-color in situ hybridization by means of a novel chromagenic substrate combination. *Dev. Dyn.* **235**, 2811-2816.

**Jain, R. K.** (2003). Molecular regulation of vessel maturation. *Nat. Med.* **9**, 685-693.

**Jande, S. S., Maler, L. and Lawson, D. E. M.** (1981). Immunohistochemical mapping of vitamin D-dependent calcium-binding protein in brain. **294**, 765-767.

**Jin, S., Hansson, E. M., Tikka, S., Lanner, F., Sahlgren, C., Farnebo, F., Baumann, M., Kalimo, H. and Lendahl, U.** (2008). Notch signaling regulates platelet-derived growth factor receptor-β expression in vascular smooth muscle cells. *Circ. Res.* **102**, 1483-1491.

**Johnson, L. R.** (2003). *Essential Medical Physiology*, 3rd edn. New York, NY: Raven Press.

**Kobayashi, A., Valerius, M. T., Mugford, J. W., Carroll, T. J., Self, M., Oliver, G. and McMahon, A. P.** (2008). Six2 defines and regulates a multipotent self-renewing nephron progenitor population throughout mammalian kidney development. *Cell Stem Cell* **3**, 169-181.

**Kobayashi, A., Mugford, J. W., Krautzberger, A. M., Naiman, N., Liao, J. and McMahon, A. P.** (2014). Identification of a multipotent self-renewing stromal progenitor population during mammalian kidney organogenesis. *Stem Cell Rep.* **3**, 650-662.

**Koss, M., Bolze, A., Brendolan, A., Saggese, M., Capellini, T. D., Bojilova, E., Boisson, B., Prall, O. W. J., Elliott, D. A., Solloway, M. et al.** (2012). Congenital asplenia in mice and humans with mutations in a Pbx/Nkx2–5/p15 module. *Dev. Cell* **22**, 913-926.

**Kuwajima, T., Sitko, A. A., Bhansali, P., Jurgens, C., Guido, W. and Mason, C.** (2013). ClearT: a detergent- and solvent-free clearing method for neuronal and non-neuronal tissue. *Development* **140**, 1364-1368.

**Leveen, P., Pekny, M., Gebre-Medhin, S., Swolin, B., Larsson, E. and Betsholtz, C.** (1994). Mice deficient for PDGF B show renal, cardiovascular, and hematological abnormalities. *Genes Dev.* **8**, 1875-1887.

**Levinson, R. S., Batourina, E., Choi, C., Vorontchikhina, M., Kitajewski, J. and Mendelsohn, C. L.** (2005). Foxd1-dependent signals control cellularity in the renal capsule, a structure required for normal renal development. *Development* **132**, 529-539.

**Lindahl, P., Johansson, B. R., Levéen, P. and Betsholtz, C.** (1997). Pericyte loss and microaneurysm formation in PDGF-B-deficient mice. *Science* **277**, 242-245.

**Magnusson, P. U., Looman, C., Ahgren, A., Wu, Y., Claesson-Welsh, L. and Heuchel, R. L.** (2007). Platelet-derived growth factor receptor-β constitutive activity promotes angiogenesis in vivo and in vitro. *Arterioscler. Thromb. Vasc. Biol.* **27**, 2142-2149.

**Mahadevan, A., Welsh, I. C., Sivakumar, A., Gludish, D. W., Shilvock, A. R., Noden, D. M., Huss, D., Lansford, R. and Kurpios, N. A.** (2014). The left-right *Pitx2* pathway drives organ-specific arterial and lymphatic development in the intestine. *Dev. Cell* **31**, 690-706.

**Marcelo, K. L., Goldie, L. C. and Hirschi, K. K.** (2013). Regulation of endothelial cell differentiation and specification. *Circ. Res.* **112**, 1272-1287.

**Olson, L. E. and Soriano, P.** (2011). PDGFRβ signaling regulates mural cell plasticity and inhibits fat development. *Dev. Cell* **20**, 815-826.

**Penkov, D., San Martín, D. M., Fernandez-Díaz, L. C., Rosselló, C. A., Torroja, C., Sánchez-Cabo, F., Warnatz, H. J., Sultan, M., Yaspo, M. L., Gabrieli, A. et al.** (2013). Analysis of the DNA-binding profile and function of TALE homeoproteins reveals their specialization and specific interactions with Hox genes/proteins. *Cell Rep.* **3**, 1321-1333.

**Potente, M., Gerhardt, H. and Carmeliet, P.** (2011). Basic and therapeutic aspects of angiogenesis. *Cell* **146**, 873-887.

**Rector, B. A.** (2007). *The Kidney*. Philadelphia: WB Saunders.

**Rodman, J., Mooseker, M. and Farquhar, M.** (1986). Cytoskeletal proteins of the rat kidney proximal tubule brush border. *Eur. J. Cell Biol.* **42**, 319-327.

**Ruan, J., Luo, M., Wang, C., Fan, L., Yang, S. N., Cardenas, M., Geng, H., Leonard, J. P., Melnick, A., Cerchietti, L. et al.** (2013). Imatinib disrupts lymphoma angiogenesis by targeting vascular pericytes. *Blood* **121**, 5192-5202.

**Saleh, M., Rambaldi, I., Yang, X.-J. and Featherstone, M. S.** (2000). Cell signaling switches HOX-PBX complexes from repressors to activators of transcription mediated by histone deacetylases and histone acetyltransferases. *Sci. Signal.* **20**, 8623.

**Sawada, H., Stukenbrok, H., Kerjaschki, D. and Farquhar, M.** (1986). Epithelial polyanion (podocalyxin) is found on the sides but not the soles of the foot processes of the glomerular epithelium. *Am. J. Pathol.* **125**, 309.

**Schrimpf, C. and Duffield, J. S.** (2011). Mechanisms of fibrosis: the role of the pericyte. *Curr. Opin. Nephrol. Hypertens.* **20**, 297-305.

**Selleri, L., Depew, M. J., Jacobs, Y., Chanda, S. K., Tsang, K. Y., Cheah, K. S., Rubenstein, J. L., O'Gorman, S. and Cleary, M. L.** (2001). Requirement for Pbx1 in skeletal patterning and programming chondrocyte proliferation and differentiation. *Development* **128**, 3543-3557.

**Sequeira-Lopez, M. L. S. and Gomez, R. A.** (2011). Development of the renal arterioles. *J. Am. Soc. Nephrol.* **22**, 2156-2165.

**Soriano, P.** (1994). Abnormal kidney development and hematological disorders in PDGF beta-receptor mutant mice. *Genes Dev.* **8**, 1888-1896.

**Srinivas, S., Watanabe, T., Lin, C.-S., William, C. M., Tanabe, Y., Jessell, T. M. and Costantini, F.** (2001). Cre reporter strains produced by targeted insertion of EYFP and ECFP into the ROSA26 locus. *BMC Dev. Biol.* **1**, 4.

**Stankunas, K., Shang, C., Twu, K. Y., Kao, S.-C., Jenkins, N. A., Copeland, N. G., Sanyal, M., Selleri, L., Cleary, M. L. and Chang, C.-P.** (2008). Pbx/Meis deficiencies demonstrate multigenetic origins of congenital heart disease. *Circ. Res.* **103**, 702-709.

**Tallquist, M. D., French, W. J. and Soriano, P.** (2003). Additive effects of PDGF receptor β signaling pathways in vascular smooth muscle cell development. *PLoS Biol.* **1**, e52.

**Tang, W. W., Ulich, T. R., Lacey, D. L., Hill, D. C., Qi, M., Kaufman, S. A., Van, G. Y., Tarpley, J. E. and Yee, J. S.** (1996). Platelet-derived growth factor-BB induces renal tubulointerstitial myofibroblast formation and tubulointerstitial fibrosis. *Am. J. Pathol.* **148**, 1169.

**Uramoto, H., Wetterskog, D., Hackzell, A., Matsumoto, Y. and Funa, K.** (2004). p73 competes with co-activators and recruits histone deacetylase to NF-Y in the repression of PDGF β-receptor. *J. Cell Sci.* **117**, 5323-5331.

**Vierstra, J., Rynes, E., Sandstrom, R., Zhang, M., Canfield, T., Hansen, R. S., Stehling-Sun, S., Sabo, P. J., Byron, R., Humbert, R. et al.** (2014). Mouse regulatory DNA landscapes reveal global principles of cis-regulatory evolution. *Science* **346**, 1007-1012.

**Vitobello, A., Ferretti, E., Lampe, X., Vilain, N., Ducret, S., Ori, M., Spetz, J.-F., Selleri, L. and Rijli, F. M.** (2011). Hox and Pbx factors control retinoic acid synthesis during hindbrain segmentation. *Dev. Cell* **20**, 469-482.

**Walls, J. R., Coultas, L., Rossant, J. and Henkelman, R. M.** (2008). Three-dimensional analysis of vascular development in the mouse embryo. *PLoS ONE* **3**, e2853.

**Weissmueller, S., Manchado, E., Saborowski, M., Morris, J. P., IV, Wagenblast, E., Davis, C. A., Moon, S.-H., Pfister, N. T., Tschaharganeh, D. F. Kitzing, T. et al.** (2014). Mutant p53 drives pancreatic cancer metastasis through cell-autonomous PDGF receptor β signaling. *Cell* **157**, 382-394.

**Zimmerhackl, L. B., Rostasy, K., Wiegele, G., Rasenack, A., Wilhelm, C., Lohner, M., Brandis, M. and Kinne, R. K. H.** (1996). Tamm-Horsfall protein as a marker of tubular maturation. *Pediatr. Nephrol.* **10**, 448-452.